Arch. Mech., **59**, 4–5, pp. 385–401, Warszawa 2007

Fast multipole boundary element method for the analysis of plates with many holes

J. PTASZNY, P. FEDELIŃSKI

Department of Strength of Materials and Computational Mechanics
Silesian University of Technology
ul. Konarskiego 18a, 44-100 Gliwice, Poland

A THREE-NODE quadratic element version of the fast multipole boundary element method (FMBEM) for two-dimensional elastostatic problems is presented. The method is applied to the analysis of perforated plates. A comparison of convergence and accuracy of the present method using quadratic elements with the method using constant elements, presented by other authors, is given. Stress results for a square plate with a circular hole are investigated. Effective material properties of plates with many holes are estimated and compared to analytical results. Implementation of quadratic-element version of the FMBEM resulted in a lower number of degrees of freedom and expansion terms, and similar accuracy to constant-element version of the method, for the same structures. Influence of boundary conditions on the convergence of the iterative solver is investigated. The effectiveness of the FMBEM in relation to the conventional BEM is presented.

Key words: elastostatics, fast multipole boundary element method, quadratic boundary element, porous material, effective material properties.

1. Introduction

THE BOUNDARY ELEMENT METHOD (BEM) is one of the efficient numerical methods being applied to analysis of mechanical structures. For a large group of problems, solutions are obtained by discretization of the boundaries only. On the other hand, analysis of structures with large number of degrees of freedom (DOF) may become uneconomical (with respect to the the solution time) or even impossible to perform (with respect to the memory). In the method, solution time and the required memory are of order $O(N^2)$, where N is the number of DOF. Such very large problems can be solved efficiently by the fast multipole BEM (FMBEM). The number of operations and memory are reduced to $O(N)$.

The fast multipole method (FMM) is applied to the analysis of potential problems with discrete or continuous field sources distribution [1, 2]. The former case refers to many-particle problems. The latter one refers to integral

equation formulations of potential problems. The FMM uses a potential expansion at the point, near to integration points (multipole expansion), for far field interactions. Thus, the terms of the corresponding potentials, resulting from many integration points, are reduced to a single point. Multipole functions are further expanded at the point near to collocation points (local expansion), and the previously reduced interactions are redistributed to many collocation points. The FMM uses also the multipole-to-multipole (M2M), the multipole-to-local (M2L), and the local-to-local (L2L) translations [1, 2].

The FMM with all the above-mentioned operations reduces the complexity of potential problem to $O(N)$. One can use only the multipole expansion, without any of the translations, to obtain the $O(N \log N)$ complexity algorithm [3].

The FMM is applied in such fields as: astrophysics, electrostatics, electrodynamics, magnetism, heat conduction, fluid mechanics, acoustics, solid mechanics and coupled problems. Look in [4] for a wide list of references on the FMBEM.

In this papers, an analysis of elastic plates with many identical circular holes, which can model a porous material, is presented. Other authors have already considered the analysis of such structures by means of the conventional BEM [5] or FMBEM [6, 7]. However, they used fast multipole codes with one-node constant boundary elements. In this work, the FMBEM with quadratic three-node elements is presented. The accuracy of the proposed method was verified for simple structures, for which analytical results are known [8]. The influence of discretization on accuracy is ivestigated. The effective Young modulus and Poisson ratio are calculated for perforated plates. The results are compared with solutions obtained by other methods. The effectiveness of the present FMBEM code is also investigated.

2. The FMBEM for 2D elastostatics

A two-dimensional, homogenous, isotropic and linear-elastic body Ω, bounded by the boundary Γ, is considered. Displacements and tractions on the boundary are given as boundary conditions. The problem is described by Somigliana's identity [9]. If there are no volume forces, it has the form of the boundary integral equation:

$$C_{ij}\left(x'\right) u_j\left(x'\right) + \int_{\Gamma} T_{ij}\left(x', x\right) u_j\left(x\right) d\Gamma\left(x\right) = \int_{\Gamma} U_{ij}\left(x', x\right) t_j\left(x\right) d\Gamma\left(x\right), \tag{2.1}$$

where T_{ij} and U_{ij} denote fundamental solutions of elastostatics, which depend on positions of the collocation point x' and the integration point x, t_j and u_j

are components of boundary tractions and displacements, and C_{ij} is a coefficient depending on position of the collocation point. The fundamental solutions have the following forms:

$$U_{ij} = \frac{1}{8\pi\mu\,(1-\nu)}\left[(3-4\nu)\ln\left(\frac{1}{r}\right)\delta_{ij} + \frac{r_i r_j}{r^2}\right], \tag{2.2}$$

$$T_{ij} = \frac{-1}{4\pi\,(1-\nu)\,r}\left\{\frac{\partial r}{\partial n}\left[(1-2\nu)\,\delta_{ij} + \frac{2r_i r_j}{r^2}\right] - (1-2\nu)\,\frac{r_i n_j - r_j n_i}{r}\right\}, \tag{2.3}$$

where μ is the shear modulus, ν is the Poisson ratio, $\mathbf{r}$ is a vector connecting the collocation point with the integration point and $\mathbf{n}$ is a unit vector, normal to the boundary at the integration point.

The boundary Γ is discretized using a certain type of boundary elements. Eq. (2.1) is applied for every boundary node as a collocation point. Thus, one obtains a system of linear equations, which can be written in the matrix form:

$$[\mathbf{H}]\,\{\mathbf{U}\} = [\mathbf{G}]\,\{\mathbf{T}\}, \tag{2.4}$$

where the matrices $[\mathbf{H}]$ and $[\mathbf{G}]$ depend on the fundamental solutions and interpolation functions of boundary quantities within the boundary elements (shape functions), $\{\mathbf{U}\}$ and $\{\mathbf{T}\}$ are vectors of boundary displacements and tractions respectively.

The matrices in Eq. (2.4) are dense and nonsymmetric. The computation time of all the entries and memory required to store them are proportional to N^2, where N is the number of DOF. For this reason, the conventional BEM can be applied to the analysis of relatively small structures. To overcome this difficulty, the fast multipole version of BEM can be applied. The algorithm has been described in detail for example in [4, 6, 7] and [11]. Only a brief description of the method, will be given here.

The integrals in Eq. (2.1) describe interactions between integration points and collocation points. The basic idea of the FMM consists in approximate calculation of the interactions between points, which are located far enough from each other. The integrals are approximated using their Taylor expansions. Let us consider a term of the single layer potential resulting from integration along elements β, located within the cluster α (Fig. 1):

$$I_{i\alpha}(x') = \sum_{\beta}\int_{\Gamma_\beta} U_{ij}\left(x', x\right) t_{j\beta}\,(x)\,d\Gamma\,(x). \tag{2.5}$$

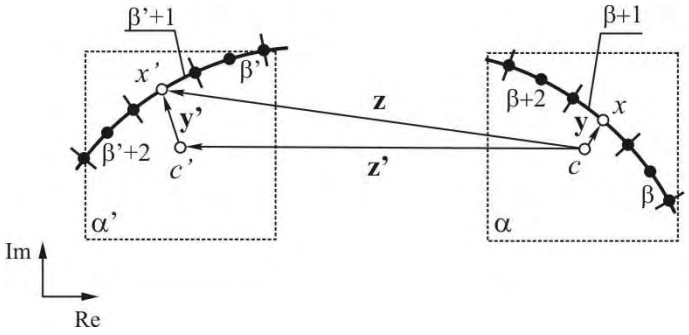

FIG. 1. Scheme of multipole and local expansions.

The point c is determined, at which the complex Taylor expansion will be constructed. The series has the following form [10]:

$$I_{1\alpha}(x') = \frac{1}{8\pi\mu(1-\nu)} \operatorname{Re}\Bigg\{ (4\nu-3) \sum_{k=0}^{\infty} f(\mathbf{z},k)\, A_{1\alpha}(k) + \sum_{k=0}^{\infty} f^{\mathrm{Re}}(\mathbf{z},k+1)\, a_{1\alpha}(k) - \sum_{k=0}^{\infty} f(\mathbf{z},k+1)\, a_{1\alpha}^{\mathrm{Re}}(k) + \sum_{k=0}^{\infty} f^{\mathrm{Im}}(\mathbf{z},k+1)\, a_{2\alpha}(k) - \sum_{k=0}^{\infty} f(\mathbf{z},k+1)\, a_{2\alpha}^{\mathrm{Im}}(k) \Bigg\},$$

(2.6)

$$I_{2\alpha}(x') = \frac{1}{8\pi\mu(1-\nu)} \Bigg\{ (4\nu-3)\ \operatorname{Re}\sum_{k=0}^{\infty} f(\mathbf{z},k)\, A_{2\alpha}(k) - \operatorname{Im}\sum_{k=0}^{\infty} f^{\mathrm{Im}}(\mathbf{z},k+1)\, a_{2\alpha}(k) + \operatorname{Im}\sum_{k=0}^{\infty} f(\mathbf{z},k+1)\, a_{2\alpha}^{\mathrm{Im}}(k) + \operatorname{Re}\sum_{k=0}^{\infty} f^{\mathrm{Im}}(\mathbf{z},k+1)\, a_{1\alpha}(k) - \operatorname{Re}\sum_{k=0}^{\infty} f(\mathbf{z},k+1)\, a_{1\alpha}^{\mathrm{Im}}(k) \Bigg\}.$$

In the expansion, functions depending on the vector $\mathbf{z}$ occur:

$$f(\mathbf{z},k) = \begin{cases} \ln(\mathbf{z}), & k=0, \\ \mathbf{z}^{-k}, & k=1,\ 2,\ ...,\ \infty, \end{cases} \tag{2.7}$$

$$f^{\mathrm{Re}}(\mathbf{z},k) = \mathbf{z}^{-k} \operatorname{Re}\mathbf{z}, \qquad f^{\mathrm{Im}}(\mathbf{z},k) = \mathbf{z}^{-k} \operatorname{Im}\mathbf{z},$$

and also the coefficients depending on the vector $\mathbf{y}$:

$$
\begin{aligned}
a_{i\alpha}(k) &= \sum_{\beta} \int_{\Gamma_\beta} \mathbf{y}^k t_{i\beta} d\Gamma(x), \\
a_{i\alpha}^{\mathrm{Re}}(k) &= \sum_{\beta} \int_{\Gamma_\beta} \mathbf{y}^k \operatorname{Re}\mathbf{y}\; t_{i\beta} d\Gamma(x), \\
a_{i\alpha}^{\mathrm{Im}}(k) &= \sum_{\beta} \int_{\Gamma_\beta} \mathbf{y}^k \operatorname{Im}\mathbf{y}\; t_{i\beta}\, d\Gamma(x), \\
A_{i\alpha}(k) &= \begin{cases} a_{i\alpha}(k), & k = 0, \\ -\dfrac{1}{k} a_{i\alpha}(k), & k = 1,\ 2,\ ...,\ \infty. \end{cases}
\end{aligned}
\tag{2.8}
$$

This type of expansion is called multipole. It is convergent, if the following condition is satisfied:

$$
y \leq \frac{1}{2} z. \tag{2.9}
$$

Thus, the far and near-fields are determined for all collocation points. The functions (2.7) are expanded further at the point c' determined for the square α', containing the collocation point (Fig. 1). This expansion is called local. It has a form similar to the multipole expansion (2.6). Definitions of local functions and coefficients can be found in [4, 6, 7] and [11]. The local coefficients can be obtained from the multipole ones by using multipole-to-local translation (M2L). We can say, that the interactions coming from integration points in the cluster α (far field) are reduced to the point c, translated to the point c', and then redistributed to many collocation points in the cluster α'.

In order to construct the expansions, one has to perform clustering of the boundary elements. First, the body Ω is enclosed within a rectangle (Fig. 2a). The rectangle is divided into four smaller ones. Each of them is divided further, until the smallest ones contain a certain number of boundary elements. All the rectangles form a boundary element clusters (Fig. 2b). The hierarchy of the clusters can be mapped using a tree structure (Fig. 2c). The root of the tree stands for the largest cluster, which contains all the boundary elements. The tree consists of nodes, their children and parents. The nodes on the highest level are called leaves. The multipole coefficients are calculated only for leaves. Then, the coefficients for their parents are evaluated using the multipole-to-multipole translation (M2M). It consists in translation of the expansion points and summation of the corresponding children's coefficients (Fig. 2a). In order

to calculate the coefficients for all the clusters, an upward pass is performed. Then, the M2L translation is performed for all the clusters. Next step is a downward pass and calculation of local coefficients for children with local-to-local translation (L2L) [4, 6, 7, 11]. Finally, the far-field terms of potentials are evaluated. The order of transformations is shown in Fig. 3. The multipole coefficients are denoted by $A_{i\alpha}(k)$, local coefficients by $B_{i\alpha}(k)$ and local functions by $g(k, y')$.

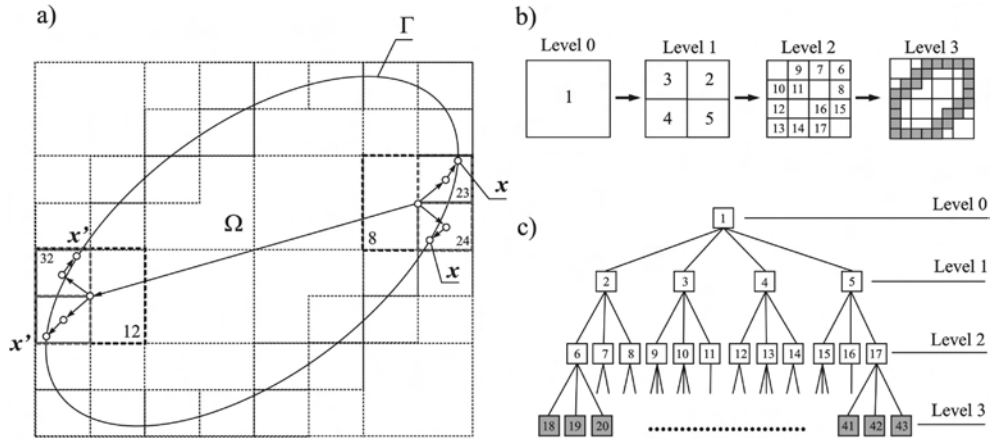

FIG. 2. Clustering of the boundary elements.

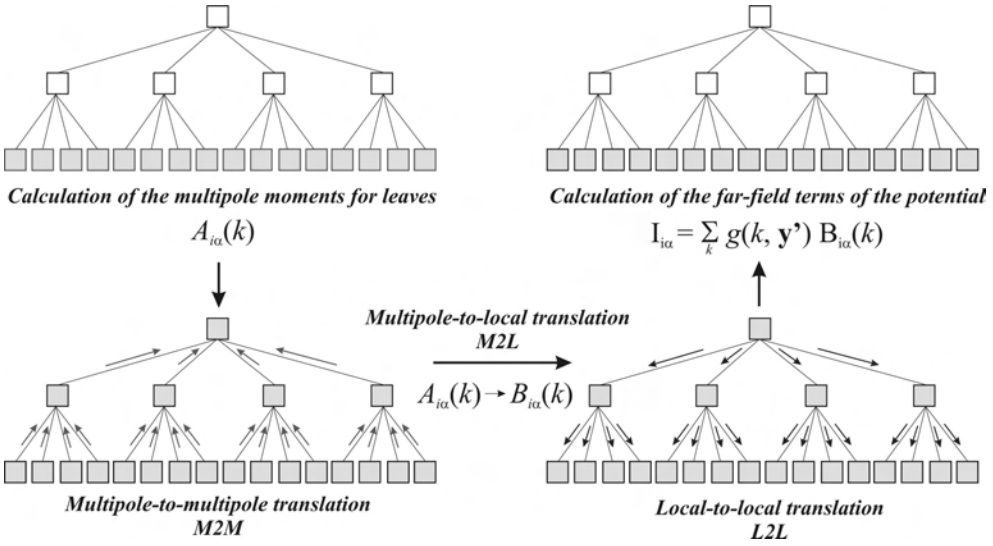

FIG. 3. The sequence of multipole coefficient transformations.

In the FMBEM, Eq. (2.4) has the following form:

$$[\mathbf{H}]^{\text{near}}\{\mathbf{U}\} + \{\mathbf{HU}\}^{\text{far}} = [\mathbf{G}]^{\text{near}}\{\mathbf{T}\} + \{\mathbf{GT}\}^{\text{far}}. \tag{2.10}$$

The terms of the far-field vectors are obtained by means of expansions. The entries of the near-field matrices are calculated directly (Fig. 4). The matrices have a block or band sparsity pattern, depending on the geometry of the structure. Modification of the system (2.10) in accordance with boundary conditions leads to a linear system of equations, which can be solved only by means of an iterative method:

$$\left\{\mathbf{AX}^i\right\} = \{\mathbf{B}\}, \tag{2.11}$$

where $\{\mathbf{X}\}^i$ denotes the approximation of the solution after the i-th iteration.

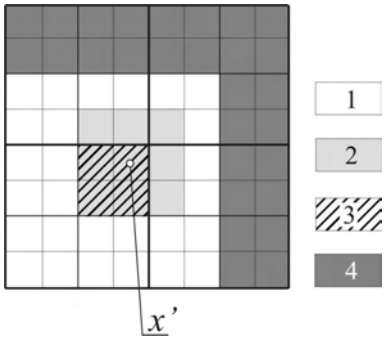

FIG. 4. Fields for the leaf x': 1 – interaction leaves (integration using expansions), 2 – near-field (direct integration), 3 – parent, 4 – interaction list for parent.

3. Numerical implementation of the FMBEM using quadratic elements

A FMBEM computer code, for analysis of 2D elastostatic problems, using quadratic three-node boundary elements is developed. Such elements model better the complex geometry, displacements and tractions of real structures than constant and linear elements. In the present code, all regular integrals are calculated using the standard 10-point Gaussian quadrature. For calculation of singular terms of the single layer potential, a special logarithmic Gaussian quadrature is used. The singular terms of the double layer potential are calculated by a rigid body movement consideration.

In the quadratic-element version of the FMBEM, the maximum number of elements in leaves can be lower than for the constant-element version. Usually

for the latter case it ranges from 20 to 40 [6, 7, 11]. In the present code, it was set to 10 or 20. For such values, the number of iterations and the computation time of the near-field contributions are reasonable. An element is assumed to be located in a cluster, if its middle node is located there. For each cluster, coordinates of expansion points are calculated as mean values of coordinates of all nodes contained in the cluster. The extreme nodes of some elements can be located outside the cluster (Fig. 5). To assure convergence of the expansions, an additional far criterion is introduced:

$$y_{\max} \leq 0.4\left(z' - y'_{\max}\right) \quad \wedge \quad y'_{\max} \leq 0.4\left(z' - y_{\max}\right). \tag{3.1}$$

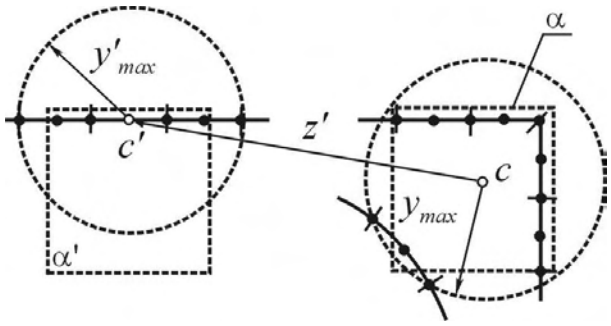

FIG. 5. A scheme for the far criterion formulation.

4. Numerical examples

4.1. Example 1. A square plate with a circular hole

In this section, a numerical example of a square plate with a circular hole at the center, under tension, is presented (Fig. 6). The same structure was analyzed by LIU in [7], using the FMBEM with constant elements. Here, the boundaries of the structure are discretized using three-node quadratic elements. The length of the edge of the plate is $a = 1\,\mathrm{m}$. The radius of the hole is $r = 0.1\,\mathrm{m}$ (it satisfies the condition $r = 0.1\,a$, as in the cited article). The material properties are as follows: Young's modulus $E = 2 \cdot 10^5\,\mathrm{MPa}$ and Poisson's ratio $\nu = 0.3$. The plate is in plain stress. The right-hand side edge of the plate is loaded by the uniformly distributed horizontal traction $p = 100\,\mathrm{MPa}$. The hoop stress σ_Θ at points A and B on the boundary of the hole is analyzed. The values are close to the analytical solution for an infinite plate with circular hole, under tension. However, the ratio r/a is too large to provide convergence to the analytical solution, which is $\sigma_\Theta^A = 3p$ and $\sigma_\Theta^B = -p$.

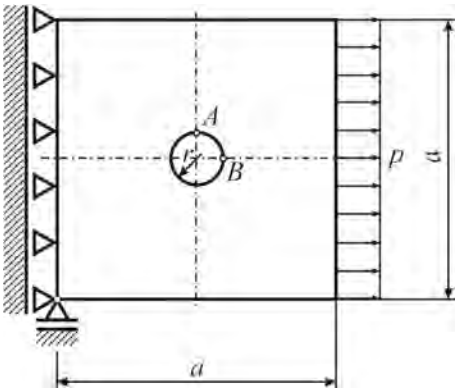

FIG. 6. A square plate with a circular hole under tension.

Six discretization schemes were considered. The number of elements used for discretization of the hole boundary was equal to 6, 8, 12, 16 and 20 respectively. For the discretization of each side of the square, 25 elements were used. For the last scheme of the hole edge discretization (20 elements), also 50 elements for each side were used. The number of degrees of freedom ranged from 424 to 880. The maximum number of elements in leaves was set to 10, except for the last case when it was set to 20. Each analysis was performed twice: for 5 and 10 terms of both the multipole and the local expansions. The system of equations was solved using the preconditioned GMRES. The initial guess was a zero vector and the tolerance for convergence was set to 10^{-6}. The preconditioner sparsity pattern was based on holes [6]. In most cases the method converged after 19 iterations. Only in the last case it converged after 21 iterations. The number of iterations was independent of the number of expansion terms. For the finest discretization scheme, also conventional BEM analysis was carried out. Table 1 shows a comparison of the results obtained by different methods. Table 2 shows all results obtained by the present method, and Fig. 7 shows the results for the hoop stress with respect to the number of DOF, obtained by different versions of the BEM.

Table 1. Hoop stresses obtained by different methods.

Method	DOF	σ_Θ^A/p	σ_Θ^B/p
FEM, 4–node quadrilateral elements, LIU [7]	38 440	3.226	−1.192
FMBEM, constant elements, LIU [7]	7 600	3.222	−1.190
Conventional BEM, quadratic elements	880	3.222	−1.190
FMBEM, quadratic elements, 5 expansion terms	880	3.229	−1.196
FMBEM, quadratic elements, 10 expansion terms	880	3.222	−1.191

Table 2. Present FMBEM results for the hoop stress.

DOF	5 expansion terms		10 expansion terms	
	σ_{Θ}^{A}/p	σ_{Θ}^{B}/p	σ_{Θ}^{A}/p	σ_{Θ}^{B}/p
424	3.211	−1.179	3.207	−1.175
432	3.224	−1.188	3.220	−1.186
448	3.225	−1.192	3.220	−1.189
464	3.226	−1.193	3.220	−1.189
480	3.226	−1.193	3.220	−1.190
880	3.229	−1.196	3.222	−1.191

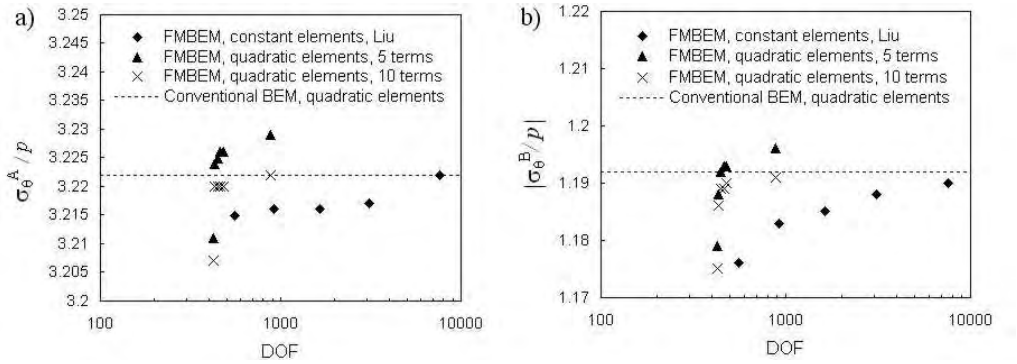

FIG. 7. The hoop stress: a) at the point A, b) at the point B.

As it was expected, much lower number of DOF is sufficient for quadratic elements than for constant ones, to achieve the same or better accuracy (Fig. 7). Also the number of expansion terms can be from 2 to even 5 times smaller. The FMBEM version with constant elements requires 20 or 25 terms [6, 7]. Both versions of the method converge within similar iteration number, which is about 20. It can be seen from Figs. 7a and 7b, that the calculated stresses converge to a higher value than the conventional BEM result, for the presented version of the method, with 5 expansion terms. For 10 expansion terms, the results coincide with the conventional BEM results as the relative difference is less than 0.1%. The small number of DOF in conjunction with small number of expansion terms can give a significant memory saving.

4.2. Example 2. Square plates with many circular holes

The second example shows an analysis of square perforated plates with different numbers of uniformly and randomly distributed identical circular holes. Two types of boundary conditions (b. c.) are considered: mixed and of traction type (Fig. 8). The effective Young modulus and Poisson ratio are evaluated and

compared to analytical results given in [12]. Once again, to compare two versions of the FMBEM (constant-element and quadratic-element version), similar structures to those, proposed in [7], were modeled. Material properties of the plate are: Young's modulus $E_0 = 2 \cdot 10^5$ MPa and Poisson's ratio $\nu_0 = 0.3$. The plate is loaded by the uniformly distributed horizontal traction $p = 100$ MPa. The structure is in plane stress. Table 3 shows dimensions of the analyzed plates, numbers of holes and number of boundary elements used in discretization. The radii of holes are equal to 0.1 m and the volume fraction in each case equals 12.56%. Structures with up to 144 holes and over 14 000 DOF were analyzed. It is known that such number of holes provides convergence of effective properties to the real ones. Also, there is no need to impose periodic displacement boundary conditions ([5, 7]) which give more accurate results. Generation process of structures containing many holes is time the consuming [5]. The procedure was simplified by the assumption that the holes are initially distributed in an uniform way, and only random variations for the locations, which assure that the holes do not overlap each other, are generated. This example shows, that such assumption gives results consistent with other models.

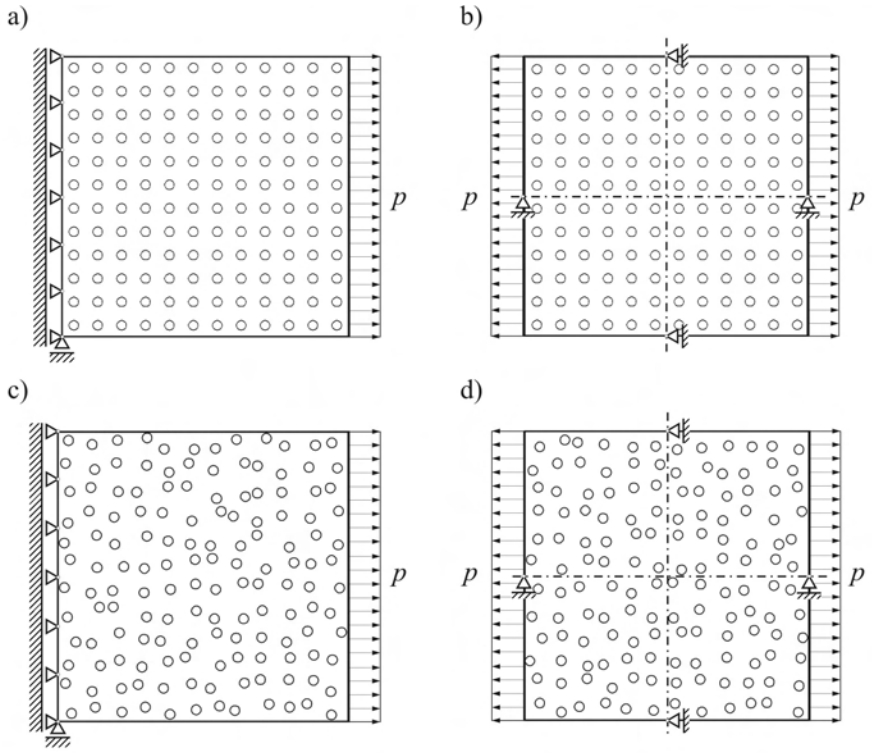

FIG. 8. Perforated plates: a) uniform distribution of holes and mixed b. c., b) uniform distribution of holes and traction b. c., c) random distribution of holes and mixed b. c., d) random distribution of holes and traction b. c.

Table 3. Geometry and discretization of analyzed structures

Number of holes	Square side length [m]	Number of elements		Total number of DOF
		per hole	per square side	
4 (2×2)	1	20 for each case	32	832
16 (4×4)	2		60	2 240
36 (6×6)	3		100	4 480
64 (8×8)	4		120	7 040
100 (10×10)	5		150	10 400
144 (12×12)	6		200	14 720

Effective Young's modulus and Poisson's ratio for each structure was evaluated and compared to analytical estimations given by KACHANOV in [12]. It corresponds to Mori–Tanaka's (MT) method. It is shown in [14] that the MT method, for relatively small volume ratios, as in this example, is compatible with other models (the self-consistent and the differential-scheme methods). It is also supported by experimental results for effective shear modulus, for volume ratios up to about 45% [12].

The system of equations was solved by the preconditioned GMRES, as in the previous example. For each analysis, the maximum number of elements in the leaf was set to 10, and the number of terms of all of expansions was set to 5.

The effective material properties are evaluated as follows:

$$E' = \frac{p}{\bar{\varepsilon}_{11}}, \qquad \nu' = \frac{-\bar{\varepsilon}_{22}}{\bar{\varepsilon}_{11}}. \tag{4.1}$$

The average strain components can be calculated as integrals along the external boundary Γ_0 of the structure [13]:

$$\bar{\varepsilon}_{ij} = \frac{1}{A} \int_{\Gamma_0} u_i n_j \, d\Gamma_0, \tag{4.2}$$

where A is the area bounded by the external boundary, u_i are the boundary displacement components and n_i are the components of the unit vector normal to the boundary ($i = 1, 2$). Table 4 shows results for the E'/E_0 ratio obtained by

Table 4. Ratio E'/E_0 obtained by different methods.

Method	Number of holes	Distribution of holes	
		uniform	random
FMBEM, constant elements, mixed b. c., LIU [7]	1 600	0.721 558	0.675 261
FMBEM, quadratic elements, mixed b. c.	144	0.719 430	0.701 290
FMBEM, quadratic elements, traction b. c.	144	0.717 300	0.697 710
Kachanov's analytical method	–	0.726 164	0.698 658

Table 5. Present FMBEM results for uniform distribution of holes.

Number of holes	Mixed boundary conditions		Traction boundary conditions	
	E'/E_0	ν'	E'/E_0	ν'
4	0.676 100	0.319 010	0.684 480	0.320 840
16	0.695 610	0.296 900	0.705 940	0.301 160
36	0.717 590	0.293 720	0.711 670	0.295 970
64	0.718 760	0.291 570	0.714 730	0.293 060
100	0.719 190	0.290 490	0.716 360	0.291 730
144	0.719 430	0.289 930	0.717 300	0.290 930

Table 6. Present FMBEM results for random distribution of holes.

Number of holes	Mixed boundary conditions		Traction boundary conditions	
	E'/E_0	ν'	E'/E_0	ν'
4	0.646 070	0.334 110	0.648 970	0.331 930
16	0.677 140	0.305 160	0.651 680	0.325 360
36	0.678 680	0.310 240	0.675 730	0.315 300
64	0.701 240	0.306 040	0.680 210	0.311 980
100	0.699 120	0.307 570	0.693 340	0.307 540
144	0.701 290	0.305 400	0.697 710	0.301 830

different FMBEM versions, compared to the analytical results. All the present results for effective material properties are shown in Tables 5 and 6. Figure 9 shows the convergence of the iterative solver with respect to the number of DOF and type of the boundary conditions.

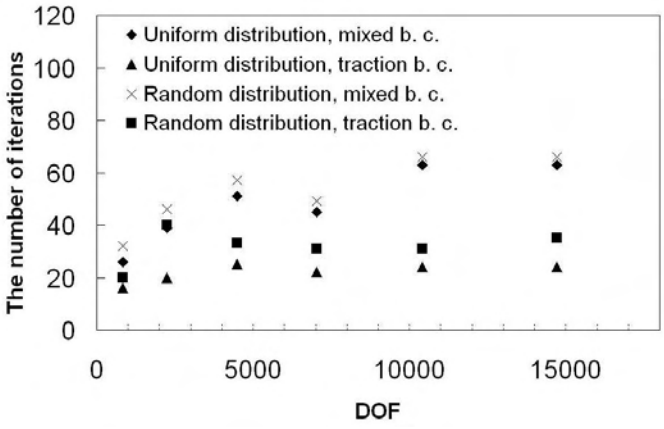

FIG. 9. Number of iterations as a function of number of DOF.

As we can see, the obtained values of apparent Young's modulus are close to the values given in References [5] and [7]. Both the values of Young's modu-

lus and Poisson's ratio are close to those determined by Kachanov's analytical method. The analytical results for E'/E_0 are given in Table 4. The results for Poisson's ratio are $\nu' = 0.309\,128$ for uniform, and $\nu' = 0.310\,045$ for random distribution of holes. As we can see, the relative difference of Poisson ratio, obtained by the FMBEM, for the case of uniformly distributed holes, is larger than for the case of randomly distributed holes.

The type of boundary conditions does not influence significantly the results. However, in this example, traction boundary conditions require smaller number of iterations than mixed boundary conditions (Figure 9). Although the structures with randomly distributed holes are nonsymmetric, the boundary condition scheme shown in Fig. 8d gives satisfactory results, and about two times smaller number of iterations, than for mixed boundary conditions, for models with 100 holes and more. It is known, that mixed boundary conditions cause a high condition number of the main matrix of the system of equations in the BEM (the system is badly conditioned). The constant-element version of the FMBEM converges faster, in spite of much larger number of DOF. For example, the number of iterations for analysis of the structure with 144 holes (108 480 DOF) and mixed boundary conditions, equals 28 [7], which is over two times less than for the method, presented here. An influence of geometry on the convergence can be also observed. For the uniform distribution of holes, the tree structure is balanced better, and the number of iterations is slightly lower, than for the random distribution.

Figure 10 shows comparison of the time of analysis for the conventional BEM and the FMBEM. The absolute computation time depends on efficiency of the facility used, accessible physical memory, programming language, etc. In

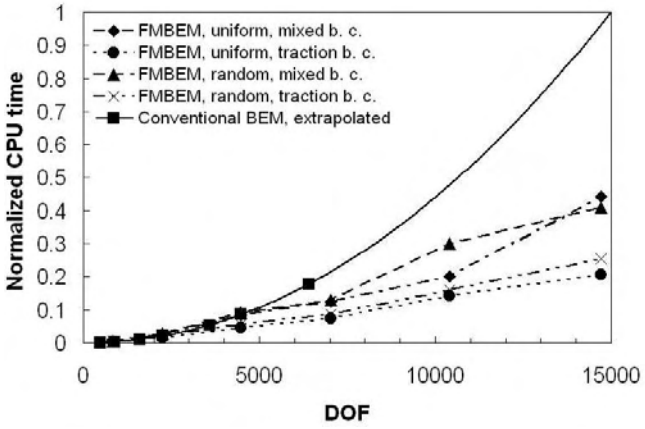

FIG. 10. Analysis time as a function of number of DOF for the conventional BEM and the FMBEM; for the FMBEM: uniform and random distribution of holes, mixed and traction boundary conditions.

Fig. 10, normalized values are given, which are related to approximate time of analysis of structure with 15 000 DOF, by the conventional BEM, using three-node quadratic elements. The conventional BEM code allowed only the analysis of structures with up to 6 400 DOF to be performed, because of memory limitation. The computation time for larger numbers of DOF was extrapolated using a quadratic function. Data points for extrapolation (whose number was equal to 7) were obtained by analyses of different structures, not included in this article. For the solution of the system of equations, Gaussian elimination was used. The efficiency of the standard BEM depends neither on the geometry nor on the boundary conditions of the analysed structure, when the system of equations is solved by a direct method.

The figure above shows that for structures with up to 5 000 DOF, the computation time of the conventional BEM and the FMBEM is similar. Making this observation, one can determine an approximate upper bound for DOF, for which the analysis can be performed efficiently by the conventional quadratic element BEM (for constant elements this limit is less than 1 000 [7]). In this context, the application of the FMBEM for analysis of structures included in Example 1, is not efficient. The example is included only to show accuracy and stability of the method.

There is a noticeable coincidence between the computation time (Fig. 10) and the number of iterations (Fig. 9) for the FMBEM. Initially, the number of iterations grows with the number of DOF, and the computation time is similar to the one of the conventional BEM. For large number of DOF, the number of iterations stabilizes and the dependence of time on DOF is close to linear. Figure 10 shows four distinct plots for the FMBEM, one for each case of geometry and boundary conditions. It is obvious that the computation time depends on the type of the boundary conditions and the geometry.

5. Conclusions

In this paper, a quadratic-element version of the FMBEM for two-dimensional elastostatics is presented. The method was applied to the analysis of perforated plates. It was demonstrated, that the number of DOF of structures discretized by quadratic elements is much smaller than for the constant element case. Stresses and displacements were investigated. The displacements were used to determine effective material properties of the perforated plates. The properties were compared to analytical estimations. The numerical results agree with the analytical ones. For the present version of the FMBEM, much lower number of expansion terms in comparison with the method using constant elements, is sufficient to provide the same accuracy [6, 7, 11]. In contradiction, the convergence of iterative process of solution of the system of equations, is better for the constant

element version. It is also shown that conditioning of the system of equations depends strongly on the type of the boundary conditions. The number of iterations can be reduced twice, for the presented structures, by replacing mixed by traction boundary conditions.

It is shown that for the present code, the FMBEM analysis is more efficient than the conventional BEM one, for structures with more than 5 000 DOF. For the constant element version the bound is less than 1 000 [7].

Small number of DOF and number of expansion terms gives a significant memory saving, in comparison to the constant element version of the FMBEM. In this work, the complex Taylor expansion given in [10] has been used. It is characterized by relatively large group of moments (4 and 5 for single and double layer potential kernels, respectively). In the Reference [7], another complex Taylor series is presented, which consists of 2 groups of moments only, for each kernel. Using this expansion with quadratic boundary elements would reduce further the memory requirements.

References

1. V. ROKHLIN, *Rapid Solution of Integral Equations of Classical Potential Theory*, J. Comput. Phys., **60**, 187–207, 1985.
2. L. GREENGARD, V. ROKHLIN, *A Fast Algorithm for Particle Simulations*, J. Comp. Phys., **73**, 325–348, 1987.
3. J. BARNES, P. HUT, *A hierarchical $O(N \log N)$ force-calculation algorithm*, Nature, **324**, 4, 446–449, 1986.
4. N. NISHIMURA, *Fast multipole accelerated boundary integral equation methods*, Appl. Mech. Rev., **55**, 4, 299–324, 2002.
5. N. HU, B. WANG, G. W. TAN, Z. H. YAO, W. F. YUAN, *Effective elastic properties of 2-D solids with circular holes: numerical simulations*, Comp. Sci. Techn., **60**, 1811–1823, 2000.
6. H. WANG, Z. YAO, P. WANG, *On the preconditioners for fast multipole boundary element methods for 2D multi-domain elastostatics*, Eng. Anal. Boundary Elements, **29**, 673–688, 2005.
7. Y. J. LIU, *A new fast multipole boundary element method for solving large-scale two-dimensional elastostatic problems*, Int. J. Numer. Meth. Engng., **65**, 863–881, 2006.
8. J. PTASZNY, P. FEDELINSKI, *Fast multipole boundary element method for two-dimensional elastostatic problems* [in Polish], Engineering Modelling, **32**, 1, 407–414, 2006.
9. J. BREBBIA, J. DOMINGUEZ, *Boundary elements an introductory course*, McGraw-Hill, New York 1992.
10. Y. YAMADA, K. HAYAMI, *A multipole boundary element method for two-dimensional elastostatics*, Tech. Report, METR 95–07, Math. Eng. Section, Dept. Math. Eng., Information Phys., Univ. Tokyo 1995.

11. Z. YAO, F. KONG, H. WANG, P. WANG, *2D Simulation of composite materials using BEM*, Eng. Anal. Boundary Elements, **28**, 927–935, 2004.

12. M. KACHANOV, *On the effective moduli of solids with cavities and cracks*, Int. J. Fracture, **59**, R17–R21, 1993.

13. V. G. KOUZNETSOVA, *Computational homogenization for the multi-scale analysis of multi-phase materials*, Technische Universiteit Eindhoven, 2002.

14. L. H. DAI, Z. P. HUANG, R. WANG, *Explicit expressions for bounds for the effective moduli of multi-phased composites by the generalized self-consistent method*, Comp. Sci. Techn., **59**, 1691–1699, 1999.

Received December 5, 2006; revised version February 12, 2007.